Mixed molybdenum oxide based partial oxidation catalyst
2. Combined X-ray diffraction, electron microscopy and Raman investigation of the phase stability of (MoVW)5O14-type oxides

M. Dieterle[1], G. Mestl[1*], J. Jäger[1], Y. Uchida[1], H. Hibst[2] and R. Schlögl[1]

[1] Department of Inorganic Chemistry, Fritz-Haber-Institute of the MPG, Faradayweg 4-6, 14195 Berlin, Germany
[2] BASF AG, ZAK/F – M301, 67056 Ludwigshafen

[*] Corresponding author: e-mail mestl@fhi-berlin.mpg.de, phone +49 30 8413 4440, fax +49 30 8413 4401

Abstract

Thermal activation of a nanocrystalline Mo_5O_{14}-type $Mo_{0.64}V_{0.25}W_{0.09}O_x$ catalyst leads to enhanced catalytic performance in the partial oxidation of methanol, propylene and acrolein. This thermal activation process was investigated by X-ray diffraction, transmission electron microscopy and Raman microspectroscopy. Thermal activation of the nanocrystalline $Mo_{0.64}V_{0.25}W_{0.09}O_x$ precursor oxide in inert atmospheres induces partial crystallization of a Mo_5O_{14}-type oxide only in a narrow temperature range ending at 818 K. The Raman spectrum of the crystalline Mo_5O_{14} oxide was identified by statistical analysis and by comparison with XRD and TEM results. The observed Raman bands in the M=O stretching mode regime were attributed to the different Mo=O bond distances in Mo_5O_{15}. A fraction of the precursor oxide remains nanocrystalline after activation as shown by Raman spectroscopy. HRTEM identified amorphous surface layers on top crystalline cores. Above 818 K, the Mo_5O_{14}-type structure disproportionates into the stable phases MoO_2 and MoO_3. This disproportionation occurs via an intermediate state which is formed by bundles of molybdenum oxide chains exhibiting structural order in only one dimension as shown by HRTEM. These results from the combined structural analysis suggest that the improvement of the catalytic performance of the MoVW oxide catalyst in the partial oxidation of methanol is related to the formation of the Mo_5O_{14} type mixed oxide.

Keywords: Selective partial oxidation, Mo_5O_{14}-type MoVW mixed oxide catalysts, Structural characterization, confocal Raman microspectroscopy, XRD, HRTEM.

Introduction

Transition metal oxides show a broad structural variety due to their ability to form phases of varying metal to oxygen ratios reflecting multiple stable oxidation states of the metal ions [1-3]. Metal oxides exhibiting strong crystallographic anisotropy may show differing catalytic properties for different exposed crystal faces. One possible reason responsible for surface structure sensitivity may be the differently strong M=O bonds at the different surface planes. The stronger the M=O bond the more basic is its function with respect to hydrocarbon activation. Other reasons for different activities may be different oxygen species on the different crystal planes, e.g. terminal, doubly, or triply bridging oxygens, generating electrophilic or nucleophilic oxidation chemistry on the different crystal planes.

Compound sensitivity can be expected in addition to this surface structure sensitivity, i.e. of all possible oxides with the overall composition $Mo_wV_{w-x}W_{w-y}O_z$ there may only be one single oxide which exhibits the highest catalytic selectivity and activity. This *compound sensitivity* may result from its special geometric, electronic or lattice diffusion properties providing selective active sites, an optimum match of catalyst and substrate electronic states and fast redox kinetics. Structure and *compound* sensitivity for oxidation reactions serve as guidelines for the development and

Mixed molybdenum oxide based partial oxidation catalyst 2. Combined X-ray diffraction, electron microscopy and Raman investigation of the phase stability of (MoVW)5O14-type oxides, M. Dieterle et al., Journal of Molecular Catalysis A: Chemical, accepted 19 January 2001

2

fundamental understanding of catalysts and their catalytic properties [4].

Haber reported that $Cu_2Mo_3O_{10}$ and $Cu_4Mo_6O_{15}$ show completely different catalytic behaviors although having identical metal stoichiometry [5]. $Cu_2Mo_3O_{10}$ is active in the isomerization and oxidative dehydrogenation of n-butene, whereas $Cu_4Mo_6O_{15}$ mainly inserts oxygen into the organic molecule to exclusively form crotonaldehyde. The only differences between these two compounds is the spatial arrangement of the atoms in the crystallographic structure and their oxidation state. Volta and coworkers examined the catalytic activity as a function of the different crystal faces of MoO_3 [6]. Samples with different ratios of (100) and (010) faces exhibited different catalytic activities. However, model studies were concentrated in most cases on pure oxides in their highest oxidation state, e.g. MoO_3 or WO_3, although these oxides are not used industrially for selective oxidation catalysis.

Intermediate molybdenum oxides, like Magnèli phases, are reported to be catalytically active for partial oxidation and may offer a way to control nature and number of catalytically active sites [7]. The phase systems of binary molybdenum, vanadium or tungsten oxides reveal a complex structural chemistry depending on the oxygen deficiency of the material [8-15]. Phase characterizations have been reported of the molybdenum oxide system mainly by X-ray diffraction (XRD) [16-21]. Transmission electron microscopy (TEM) has been used too to characterize intermediate oxide phases formed in situ by irradiating molybdenum oxide in the electron beam [22,23].

According to Kihlborg et al. [24], Mo_5O_{14} is formed by tempering an appropriate mixture of molybdenum compounds with the overall oxygen stoichiometry of 2.8 for ten days in the temperature range of 773 K to 823 K. Kihlborg, however, did not succeed to prepare pure Mo_5O_{14}. The product was always accompanied by Mo_4O_{11}, $Mo_{17}O_{47}$ and MoO_2. Mo_5O_{14} only formed in a narrow temperature interval around 773 K and decomposed upon prolonged heating [24]. The Mo_5O_{14} framework is deduced from the MoO_3 framework [20] by the introduction of pentagonal tunnels. Hyde and O'Keefe described the formation of the pentagonal tunnels by the variation of an ordered array of rotational axes in a two-dimensional superlattice of the MoO_3 framework as shown in Scheme 1 [25]. Upon this variation, a square group of four corner-sharing octahedra is rotated through $\pi/4$ radians (Scheme 1, dark polyhedra). This changes the nine square tunnels into one hexagonal, three pentagonal, four triangular and one square tunnel. One of the formed pentagonal tunnels in each rotation group is occupied by a transition metal cation. Alternatively, the formation of Mo_5O_{14} may be understood as a nucleation of anion vacancies in cylindrical (rotational) shear planes, the pentagonal tunnels [9]. As a result, the Mo_5O_{14} structure can be described as a network, built up by MoO_6 polyhedra and MoO_7 pentagonal bipyramids mutually connected by sharing corner and edges [25]. The pentagonal bipyramids share the pentagonal edges with five MoO_6 polyhedra, forming unusual groups. These
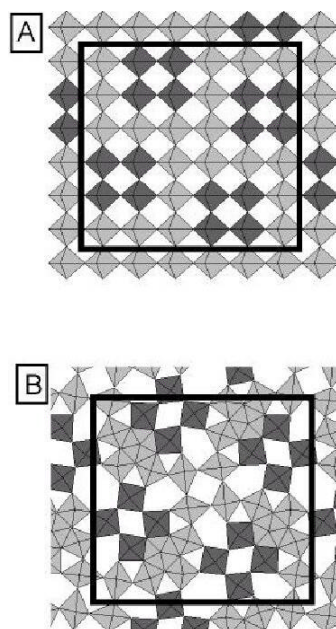
Scheme 1 Crystal structures of MoO_3 (A) and Mo_5O_{14} (B)

groups are also found in compounds like $Mo_{17}O_{47}$ [26], or $W_{18}O_{49}$ belonging all to the same structural family [27]. Kihlborg described Mo_5O_{14} as a two-dimensionally disordered oxide [24].

Molybdenum oxide based catalysts additionally contain varying minor amounts of Vb and VIb transition metals like vanadium [28, 29], tungsten [30-34], Nb [35], and/or Ta [36]. In addition to the overwhelming variety of binary intermediate oxides, ternary, and quaternary mixed molybdenum, tungsten and vanadium oxides exist too. The chemistry of all these transition metal oxides is dominated by their site preference, redox properties and their d-wave function extension [1]. As a result of the incorporation of additional elements, the Mo_5O_{14} structure is stabilized up to its melting point [36], while the binary Mo_5O_{14} already decomposes at temperatures below 823 K [13]. In this context, it is important to note that the elemental compositions of the mixed oxides $(Mo_{0.92}V_{0.08})_5O_{14}$ or $(Mo_{0.75}W_{0.25})_5O_{14}$ are close to that of industrial catalysts [8,37].

The catalyst investigated in this study has an overall composition of $Mo_{0.64}V_{0.25}W_{0.09}O_x$ [37]. Nanocrystalline Mo_5O_{14}–like oxide was mainly observed after calcination of the precursor polyoxometalate at 673 K under nitrogen [37]. Thermal activation of this material leads to a superior catalytic performance in the partial oxidation of methanol [37]. The catalytic activity increased by a factor of 3 with a selectivity increase from 66% to 88 %. This enhanced catalytic performance was correlated with a reduction of the catalyst bulk and surface. Furthermore, it was suggested that the active catalytic material consists of core of a crystalline Mo_5O_{14}–type mixed oxide and a surface layer of different stoichiometry but yet unknown structure.

In the present study, the quaternary Mo_5O_{14}-type oxide was activated at different temperatures in order to obtain information about the complex and still not well understood thermal properties and the phase stability of this compound

Mixed molybdenum oxide based partial oxidation catalyst 2. Combined X-ray diffraction, electron microscopy and Raman investigation of the phase stability of (MoVW)5O14-type oxides, M. Dieterle et al., Journal of Molecular Catalysis A: Chemical, accepted 19 January 2001

3

by XRD, high resolution transmission electron microscopy (HRTEM), and Raman microspectroscopy investigations.

Experimental

Preparation of MoVW mixed oxides

Aqueous solutions of ammonium heptamolybdate (AHM), ammonium metatungstate (AMT), and ammonium metavanadate (AMV) having the respective transition metal concentrations were mixed in order to obtain the catalyst with a composition of Mo, W and V of 64%, 9%, and 27%, respectively. This solution was dried by evaporation and decomposed under nitrogen at 673 K [38,39]. The obtained bluish black compound was used as a solid precursor for the structural investigations [8,37], and will be referred to as the starting material.

The thermal activation treatments have been carried out in a quartz tubular flow reactor (i.d. 8 mm) in the temperature range of 673 K to 829 K in a flow of 100 ml/min pure nitrogen for 1 or 2 hours. The temperature difference between the specimen location in the reactor and the reactor oven was measured prior to the experiments and the corrected temperatures are reported. The accuracy of the indicated temperatures is $\pm 1°C$.

X-ray Diffraction

All XRD measurements were made on a STOE STADI-P focusing monochromatic transmission diffractometer (Ge primary monochromator, Cu-Kα_1 radiation), equipped with a position sensitive detector (PSD) at room temperature. The phase analysis was done with the PCW 2.2 software package [40] using Retrieve single crystal data (ICSD-PDF-2).

Transmission Electron Microscopy

Specimen for electron microscopy have been prepared by the standard powder preparation technique. A small amount of oxide powder was crushed in corundum mortars to a finer powder if necessary. This specimen powder was dispersed in a neutral organic solvent, usually n-pentane, by ultrasonic stimulation. A small droplet of such a suspension, typically several μl, was brought on a copper grid covered by a carbon microgrid.

Samples were analyzed by a Philips CM 200 FEG electron microscope using a side-entry double-tilt specimen holder. The electron microscopy observations can be classified in different stages. Observations with relatively low magnifications obtain the morphological information of the specimen. Crystallographic information of small particles in the specimen can be obtained by recording their electron diffraction patterns using the selected area electron diffraction technique (SAED). A similar information was obtained by taking the lattice images.

Irradiation damage of the oxide specimens is one of the largest problems of this technique [7], because MoO$_3$ crystals and the related intermediate Mo oxides are very sensitive to electron irradiation. Therefore special care has been taken to minimize irradiation damage by applying fast image acquisition.

Confocal Raman microspectroscopy

All Raman spectra were recorded with a DILOR LABRAM I spectrometer equipped with a confocal microscope (Olympus, 100x objective) and a computerized XY-table. Raman mapping of samples can be conducted with a lateral resolution of 0.7 μm. Laterally varying sample structures can be identified on a micrometer scale by Raman imaging and related to inhomogeneous sample compositions [37]. The spectrometer is equipped with a CCD camera (1024*298 pixels), which is peltier-cooled to 243 K to reduce thermal noise. A HeNe-laser (632.8 nm, Melles Griot) operating at 1.4 mW was used for the excitation of the Raman spectra. A notch filter was applied, to cut off the laser line and the Rayleigh scattering up to about 150 cm^{-1}. The applied slit width was set to 200 μm giving a spectral resolution of 2.5 cm^{-1}. Each spectrum shown is the addition of two accumulations each integrated for 150 sec.

In order to compare large Raman data sets, statistical analysis of the principal spectral components is a prerequisite. *Simpl*e to use *i*nteractive *s*elf-modeling *m*ixture *a*nalysis (SIMPLISMA) [41,42] was used to derive the linearly independent Raman spectral components of the data set. The statistical analysis was applied to a set of 500 Raman spectra in total built by five subsets of 100 laterally resolved Raman spectra recorded of the samples thermally activated at 673, 803, 813, 818 and 829 K, respectively.

Results

XRD

Figure 1 shows the XRD patterns recorded of the oxide phases obtained by thermal activation of the starting material. The XRD pattern of the starting material (Fig. 1a) can be understood as a mixture of a majority of nanocrystalline Mo$_5$O$_{14}$-type oxide with minor amounts of nanocrystalline MoO$_3$-type material [8,37].

Mainly the Mo$_5$O$_{14}$-type oxide crystallized after thermal activation in the narrow temperature range between 803 K and 813 K (XRD reflections indicated by (+) in Fig. 1b,c). Crystalline Mo$_5$O$_{14}$-type oxide formed almost quantitatively at the activation temperature of 818 K (Fig. 1d). Monoclinic MoO$_2$- (XRD reflections indicated by (#) in Fig 1) and orthorhombic MoO$_3$-like phases (XRD reflections indicated by (*) in Fig. 1) were additionally observed. In general, MoO$_3$- and MoO$_2$-like compounds increasingly crystallize with higher temperatures.

Activation temperatures higher than 823 K led to an almost quantitative decomposition of the Mo$_5$O$_{14}$-type compound (Fig. 1e). The main decomposition products were orthorhombic MoO$_3$-like, MoO$_2$-like and X-ray amorphous oxides at activation temperatures above 823 K. The decomposition of this Mo$_5$O$_{14}$-type oxide may, therefore, be understood as a disproportionation of the metastable Mo$_5$O$_{14}$-type phase into the thermodynamically stable

Mixed molybdenum oxide based partial oxidation catalyst 2. Combined X-ray diffraction, electron microscopy and Raman investigation of the phase stability of (MoVW)5O14-type oxides,
M. Dieterle et al., Journal of Molecular Catalysis A: Chemical, accepted 19 January 2001
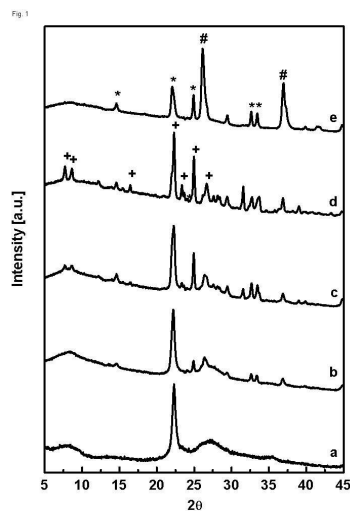
4

phases MoO_2 and MoO_3, and an X-ray amorphous mixed oxide.

Figure 1 XRD pattern of the starting material and catalysts activated at temperatures indicated: a.) starting material, b) 803 K, c.) 813 K, d.) 818 K, e.) 823 K. The reflections of Mo_5O_{14} (+), MoO_2 (#) and MoO_3 (*) are indicated.

The lattice constants of the MoO_3-like oxide (a = 4.217 Å; b = 13.458 Å; c = 3.951 Å) exhibit contractions of the a- and c-axis, while an elongation of the b-axis is observed in comparison to pure MoO_3 (Pbmn, a = 3.964 Å, b = 13.863 Å, c = 3.699 Å, β = 120.9) [20]For the MoO_2-like oxide (a = 5.611 Å; b = 4.856 Å; c = 5.317 Å), the comparison with pure MoO_2 (P21/c, a = 5.610 Å, b = 4.857 Å, c = 5.626 Å, β=120.9) [43] reveals a contraction of the a-axis and an elongation of the c-axis. These changes of the lattice parameters are probably due to the incorporated tungsten and vanadium. The lattice parameters of the Mo_5O_{14}–like oxide (a = 22.826 Å, c = 3.983 Å) are in good agreement with literature data of V substituted Mo_5O_{14} [28,29] or calculated data.[37]

A quantification of the overall phase compositions of these thermally activated samples was not possible due to the remaining nanocrystalline Mo_5O_{14}–type oxide in the samples, which was indicated by the rather high X-ray amorphous background. However, in an attempt to further understand the changes in the crystallinity, the integral intensity ratios of the X-ray amorphous background and the observed diffraction peaks normalized to the internal Si standard were evaluated to gain information about the change in the degree of crystallization with treatment temperature. The result of this estimation is shown in Fig. 2. As mentioned, the starting material was X-ray nanocrystalline. Upon thermal treatment, the X-ray nanocrystalline part of the sample diminished. About 30 %, 20 %, 5%, and 2 % remained X-ray nanocrystalline in the samples activated at 803 K, 813 K, 818 K and 823 K, respectively. Between 80 to 90 % of the crystalline material within the samples treated at temperatures below 818 K consisted of crystalline

Mo_5O_{14}–like oxide. The remaining 10 to 20 % of crystalline material comprise minor amounts of orthorhombic MoO_3-like and monoclinic MoO_2 oxides. After activation at 823 K, the amount of Mo_5O_{14}-type oxide has decreased to 40%, whereas the portions of MoO_3- and MoO_2-type oxides amount to 43 and 17%, respectively, indicating the disproportionation of Mo_5O_{14}.
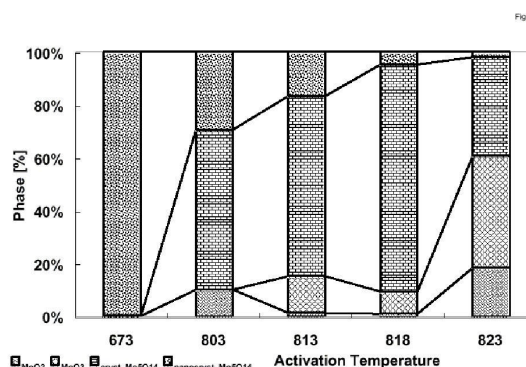

Figure 2 Quantitative XRD phase analysis of the crystalline parts of the mixed oxide catalysts activated at different temperatures

HRTEM

The starting MoVW mixed oxide material

The starting material has been thermally treated at 673 K. This temperature leads to complete decomposition of the ammonium oxometalate precursor as shown by the complete absence diffraction patterns of the precursor components (see XRD). The mixed oxides appear as black powders and their particle size distribution is between 0.1 μm and a few microns as determined by SEM [37]. TEM did not indicate the presence of well-crystallized particles (images not shown).

MoVW mixed oxides activated at 803 K for 2h

The MoVW mixed oxide which was activated at 803 K for 2 h in flowing nitrogen started to crystallize as shown by XRD. Transmission electron microscopy observations revealed that the specimen contained at least two different types of particles. Electron micrographs and diffraction patterns of the relatively large, nanocrystalline particles and the typical aggregates of very small crystalline particles are shown in Fig. 3a and 3b, respectively. The relative amount of the nanocrystalline particles is much larger than that of the aggregates of crystalline particles. These different types of particles can hardly be distinguished by a simple morphological SEM observation. Electron diffraction patterns shown in Fig. 3a exhibit relative broad diffraction rings. The first diffraction ring corresponds to a lattice spacing of about 0.42 nm. The mean particle size is estimated to be about 5 nm. Further diffraction rings correspond to the lattice spacings of 0.32 - 0.35, and 0.17 - 0.21 nm, respectively. Therefore, a complete periodic character of the materials in the

Mixed molybdenum oxide based partial oxidation catalyst 2. Combined X-ray diffraction, electron microscopy and Raman investigation of the phase stability of (MoVW)5O14-type oxides, M. Dieterle et al., Journal of Molecular Catalysis A: Chemical, accepted 19 January 2001
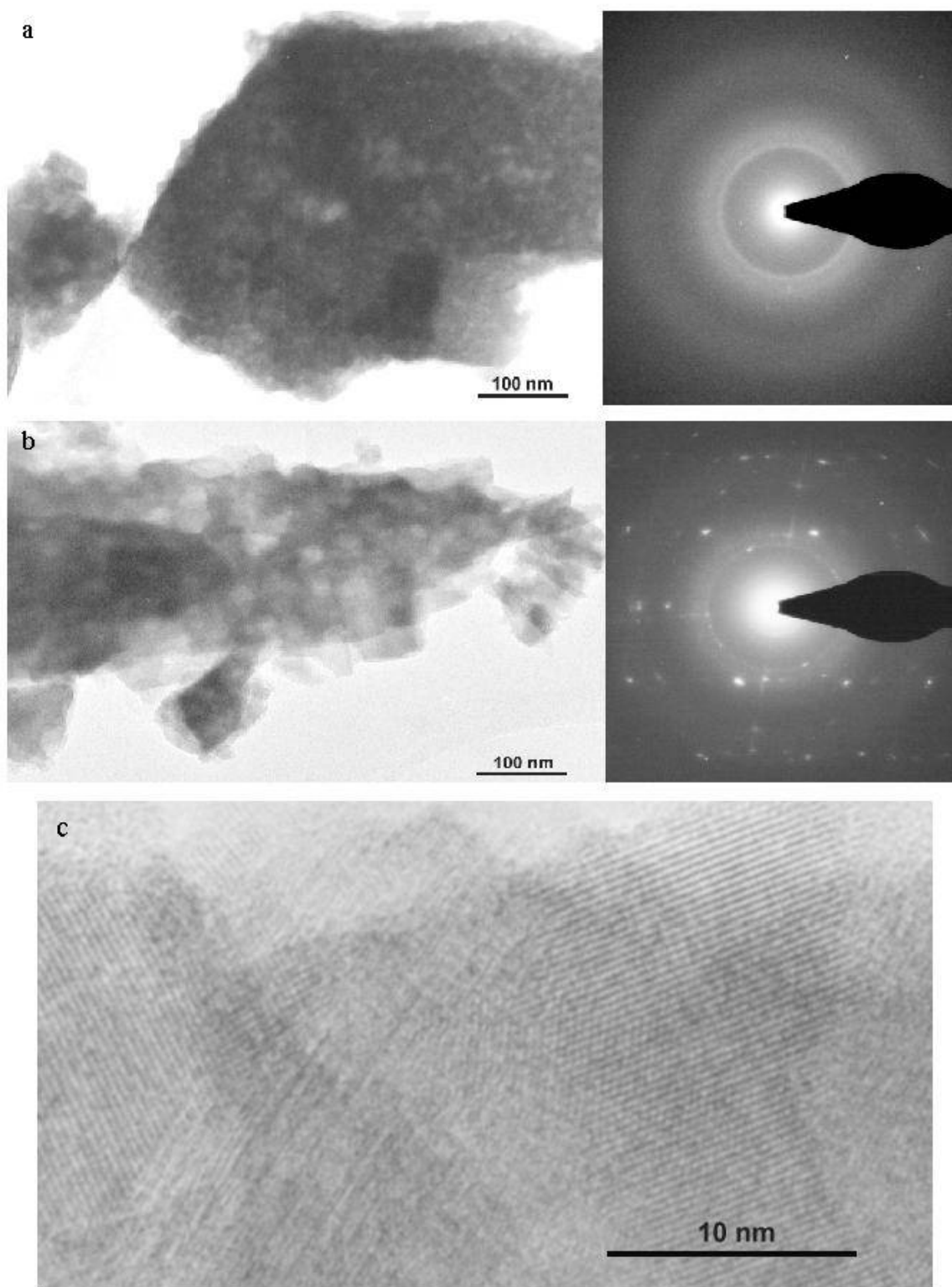
5

Fig. 3

Figure 3 Electron micrographs and diffraction patterns of the mixed oxide activated at 803 K for 2h: a) amorphous particles and selected area electron diffraction (SAED). b) aggregates of crystalline particles and SAED pattern. c) Lattice images obtained from crystallized particles.

Mixed molybdenum oxide based partial oxidation catalyst 2. Combined X-ray diffraction, electron microscopy and Raman investigation of the phase stability of (MoVW)5O14-type oxides, M. Dieterle et al., Journal of Molecular Catalysis A: Chemical, accepted 19 January 2001

6

specimen can be excluded from this electron diffraction pattern. Resolved lattice images could not be obtained of these type of nanocrystalline particles.

On the other hand, the diffraction patterns recorded of the aggregates of the crystalline particles exhibit typical diffraction spots, as shown in Fig. 3b. The average size of these small crystallite particles was estimated to be about 10 - 15 nm. The individual crystallite particle is, therefore, too small to be manipulated in the electron microscope in order to determine its crystal structure. An image of resolved lattice planes has been observed at the edge of the small aggregate shown in Fig. 3c (marked by the arrow). Almost all lattice spacings were determined to be 0.42 nm. This value fits well to the expected lattice constants of Mo_5O_{14}.

Mixed oxides activated at 813 K for 2h
The structure of the MoVW mixed oxide which was activated at 813 K for 2h has not much changed as compared to that of the mixed oxide which was activated at 803 K for 2 h, except that the nanocrystalline particles are further crystallized. As shown in Fig. 4a, a distinct lattice image can be obtained of such particles.
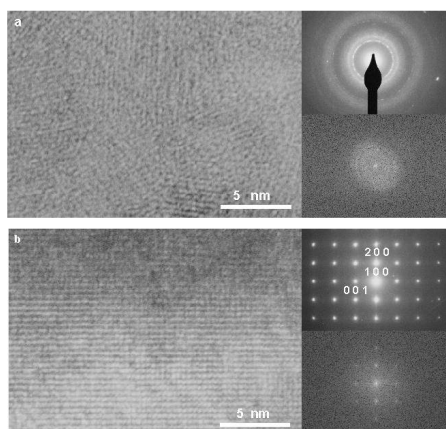

Figure 4 Electron micrographs and SAED patterns of the mixed oxide which was activated at 813 K for 2 hours. Power spectra calculated from the electron micrographs are sown below the SAED patterns. a) amorphous particles. b) MoO_3-type particle observed in the (010) crystal plane.

This tendency of an improved crystallinity is more clearly recognized in the electron diffraction patterns. The lattice spacings were estimated from the electron diffraction pattern to be 0.42, 0.34, 0.27(vw) and 0.21 nm. The optical diffraction pattern from the electron micrograph, the so-called power spectrum, is displayed below the diffraction pattern in Fig. 4a. In Fig. 4b, an electron micrograph taken at high magnification shows a two-dimensional lattice image. The diffraction pattern of this particle is very similar to that of MoO_3 oriented in the [010] direction with the exception of showing some forbidden diffraction spots such as 100, 001, etc. The extinction laws for the individual diffraction spots do not satisfy those of real MoO_3. Such a violation of the extinction law is often observed for mixed crystals and for electron irradiated MoO_3, but still the crystal structure of this particle is of the MoO_3 type.

Mixed oxides activated at 818 K for 2h
The MoVW mixed oxide catalyst was further crystallized after this activation step to form different variants. Crystalline particles, as shown in Fig. 5a, are of the orthorhombic MoO_3-like type. Fig 5b shows the lattice resolved image of a Mo_5O_{14}-type crystal in agreement with previous work [8,37].
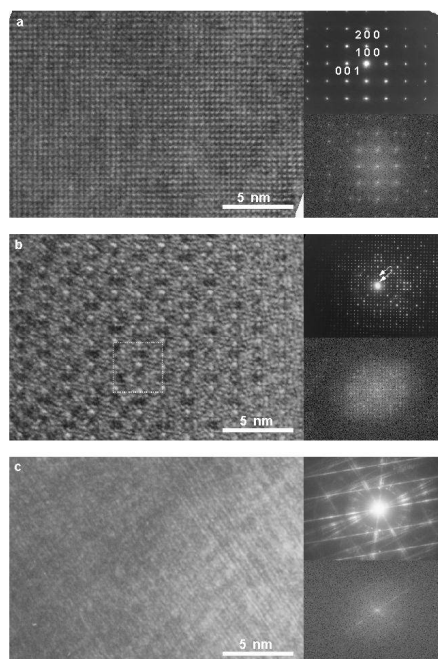

Figure 5 Electron micrographs and SAED patterns of the mixed oxide which was activated at 818 K for 2 hours. Power spectra calculated from the electron micrographs are sown below the SAED patterns. a) MoO_3-type particle observed in the (010) crystal plane; b) Mo_5O_{14}-type particle observed in the (001) crystal plane. The projected unit cell is schematically drawn in the micrograph. Forbidden diffraction spots are indicated by arrows in the SAED pattern; c) "bundle structure" type particle.

The white dotted square frames the unit cell of Mo_5O_{14}. The resolution of this electron micrograph is limited due to unfavorable defocusing and a small miss-orientation of the crystal to the incident electron beam. Arrows in Fig 5b indicate the 100, 300. etc. electron diffraction spots in the diffraction

pattern of the Mo_5O_{14} lattice in spite of the forbidden diffraction spots for Mo_5O_{14} crystals. This observation indicates again the presence of the additional V, W atoms and/or oxygen defects due to beam exposure.

More importantly, MoVW mixed oxides of another structure were additionally detected in this specimen. An electron micrograph and the electron diffraction pattern of this respective structure are shown in Fig. 5c. It can be deduced from this micrograph and the SAED pattern that this peculiar type of an MoVW mixed oxide has a fiber structure with irregular stacking of the basic structural units, the fibers. This irregular ordering is recognized from the streaks in the diffraction pattern which remained unchanged for any tilting angle. It indicates that this structure consists of chains/bundles of Mo polyhedra which show ordering only along their axis. Therefore, this peculiar structure is termed "bundle" structure (Scheme 2).
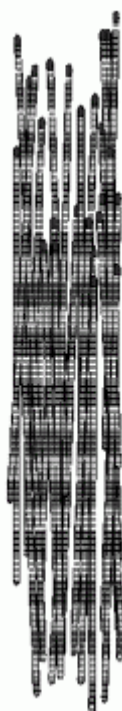
Scheme 2 Schematic drawing of the "bundle" structure of disordered bundles of chain-like molybdenum oxide oligomeres.

This observation is important with respect to the formation of MoO_3 which is observed after activation at 823 K. MoO_3 is built up by chains of MoO_4 polyhedra which are condensed to form layers. The chains or "bundles" observed by TEM thus may indicate the starting reorganization of the Mo_5O_{14}-type oxide and its recrystallization to MoO_3.

Moreover, Figure 6 shows high resolution TEM images of mixed oxide crystals whose surfaces were partly oriented parallel to the electron beam. In Fig. 6a, a Mo_5O_{14}-type oxide crystal is shown. The dotted square indicates the unit cell comparable to that in Fig. 5b. Important to note is the fringed appearance of the crystal edge, which has lost structure compared to deeper laying zones exhibiting the Mo_5O_{14} unit cell. In Fig. 6b, a well-crystallized MoO_3-type oxide crystal is shown irradiated along the [010] direction. The fringed structure of the MoO_3-type crystal edge is thinner as compared to that of the Mo_5O_{14}-type crystal but also recognized. In this case, the roughness of the crystal surface is not only seen at the edge of the crystal but also at its surface perpendicular to the beam as indicated by the mosaic contrast variations. These observation are in line with the reported combined XPS/ISS/RBS results [37] which already indicated different compositions of surface-near layers and the bulk volume. It should be noted that the information depth of XPS is about 5 nm comparable to the fringed edge of the Mo_5O_{14} crystal. Thus, it can be concluded that the catalyst particles have a core-shell structure as already suggested in the previous paper [37].
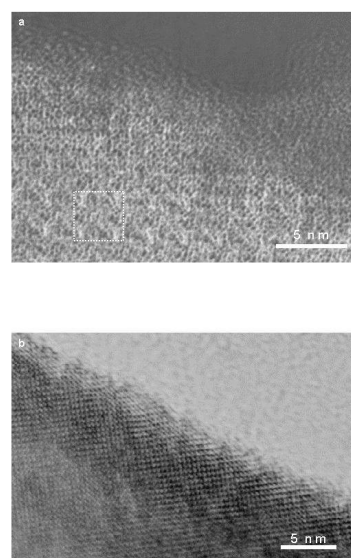
Fig. 6

Figure 6 High resolution electron micrograph of the fringed crystal edge of a crystalline Mo_5O_{14}-type particle a) and a crystalline MoO_3-type particle in the mixed oxide sample which was activated at 818 K.

Mixed oxides activated at 823 K for 2h
After this activation treatment, the MoVW mixed oxides are further crystallized. Rather small Mo_5O_{14}-type crystals (5-10 nm) but large orthorhombic MoO_3-type crystals are found. Fig. 7 shows the electron microscopic image and the diffraction pattern of one characteristic MoO_3-type crystal taken at high magnification. The morphological structure of the MoO_3 crystallite surface can be seen in addition to the two-dimensional lattice image. The crystal surfaces exhibit atomic steps formed by small islands or intrusions, as recognized by the small difference of the crystal contrast. This observation compares with the one of the fringed edge when the crystal surface is oriented parallel to the beam (Fig. 6)

Mixed molybdenum oxide based partial oxidation catalyst 2. Combined X-ray diffraction, electron microscopy and Raman investigation of the phase stability of (MoVW)5O14-type oxides, M. Dieterle et al., Journal of Molecular Catalysis A: Chemical, accepted 19 January 2001

8

and points to a disordered surface-near layer on top a crystalline core in line with the suggested core-shell model [37]. Crystals of the MoO_2 type have not been observed. This is due to the small concentration of rather large, well crystallized MoO_2 in the sample as proven by XRD (Fig. 1e) and Raman (vide infra). Particles or crystallites showing the "bundle" structure were not observed after this treatment. This can be explained by the assumption, that the bundle structure is an intermediate in the disproportionation process of the Mo_5O_{14}–like oxide to MoO_3-like and MoO_2-like oxides as shown by XRD and Raman (vide infra).
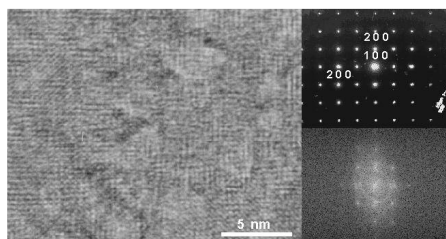
Fig. 7

Figure 7 Electron micrograph of a MoO_3-type crystal in the oxide specimen activated at 829 K for 2 hours. SAED pattern of the particle oriented in the [010] direction. The power spectrum calculated from the electron micrograph is shown below the SAED pattern.

Raman Spectroscopy

XRD and HRTEM analysis revealed that all differently activated MoVW mixed oxides contain considerable amounts of nanocrystalline, ill-defined material. Raman spectroscopy is more sensitive to nanocrystalline or amorphous substances than XRD and was therefore used to hopefully better understand the molecular structure and coordination symmetry of this nanocrystalline material. Figure 8 shows the characteristic Raman spectra of the series of thermally activated samples. The Raman spectrum of the starting material (Fig. 8a) exhibits broad Raman bands at about 930, 830, and 705 cm^{-1}. These ill-defined Raman bands are attributed to the mixture of nanocrystalline Mo_5O_{14} –type and nanocrystalline MoO_3-type compounds as already discussed in detail in the previous paper [37].

The Raman spectrum of the sample thermally activated at 803 K (Fig. 8b) is characterized by Raman bands at 990(vw

br), 908, 850, and 745 cm^{-1}, the sample activated at 813 K exhibits Raman bands at 975(sh), 902, 860(sh), 844, and 718 (sh) cm^{-1} (Fig. 8c), and the one activated at 818 K shows Raman bands at 975(sh), 902, 844, 775(sh,vw), 718 and at 685(sh,vw) cm^{-1} (Fig. 7d), and at 577, 385, 347, 336, 278, 247 cm^{-1}(not shown). With increasing activation temperature, the Raman bands become more resolved and shift to lower frequencies (Fig. 4b-5d) (compare also the Raman result shown in the previous publication [37]).
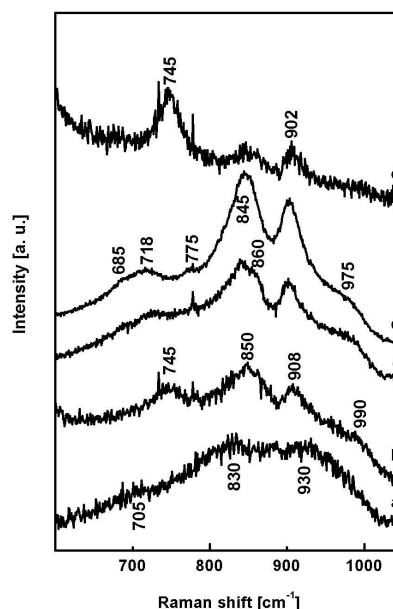
Fig. 8

Figure 8 Raman spectra of the starting material and the samples thermally activated at the temperatures indicated: a.) starting material, b) activated at 803 K, c.) activated at 813 K, d.) activated at 823 K, and e.) activated at 829 K.

After thermal activation at 829 K, above the disproportionation temperature of the Mo_5O_{14}-type oxide as determined by XRD, Raman bands are detected of monoclinic MoO_2 at 745, 596, 575, 498, 461, and 363 cm^{-1} (Fig. 8e) and of orthorhombic MoO_3 (spectrum not shown) in agreement with XRD (Fig. 1). The Raman signals of the Mo_5O_{14} –type oxide at 844 and 902 cm^{-1} have lost most of their intensity but still can be seen.

In order to account for sample inhomogeneities [37], Raman images of 100 spectra were recorded of all differently activated samples over an area of 900 μm^2 with a lateral resolution of 0.7 μm. i.e. one spectrum per 10 μm^2. Raman spectra of MoO_3-type oxide have not been included in the statistical evaluation of the Raman data, due to the extremely high Raman cross section of well-crystallized MoO_3 which would completely overwhelm all additional Raman information.

Fig. 9 shows the spectrally pure Raman components as determined by SIMPLISMA analysis of the whole set of 500 Raman spectra, i.e. 100 spectra and 5 samples. Three different spectral components can be distinguished. The first pure component resembles the typical Raman spectra of mono-

Mixed molybdenum oxide based partial oxidation catalyst 2. Combined X-ray diffraction, electron microscopy and Raman investigation of the phase stability of (MoVW)5O14-type oxides,
M. Dieterle et al., Journal of Molecular Catalysis A: Chemical, accepted 19 January 2001

9

clinic MoO_2 with spectral features at 745 cm^{-1} (Fig. 9a) and 549, 499, 462 and 364 cm^{-1} (not shown). The second pure spectral component (Fig. 9b) exhibits features at 945, 880, and 830 cm^{-1} and resembles typical Raman spectra of oligomeric molybdenum oxide clusters, comparable to hepta- or octamolybdates [44,45].
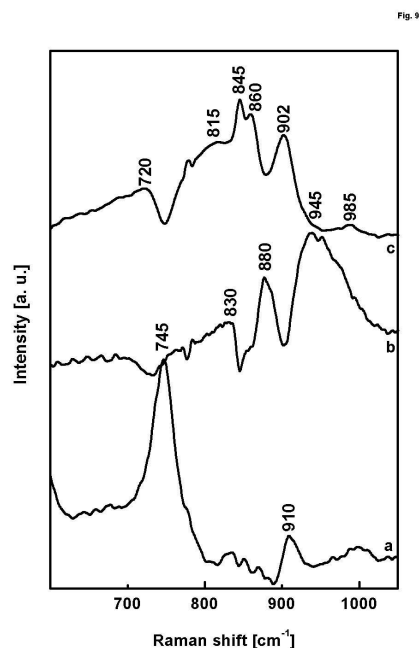

Figure 9 Spectral components according to the SIMPLISMA analysis of the set of 500 Raman spectra: a.) MoO_2-like oxide, b.) amorphous Mo_5O_{14}-type oxide, and c.) Mo_5O_{14}-type oxide.

Hence, it may be concluded that the second pure spectral component of this set of Raman spectra is due to oligomeric MoVW oxide clusters in structural analogy to polyoxometalates. These oligomeric MoVW clusters are identified with the material being responsible for the X-ray amorphous background. The third pure spectral component (Fig. 9c) resembles crystallized Mo_5O_{14}–type oxide with spectral features at 902, 860, 845, and 720 cm^{-1}, with minor contributions of nanocrystalline MoO_3-type oxide with spectral features at 985, and 815 cm^{-1}. The broad ill-defined feature at 815 cm^{-1} and the weak feature at about 985 cm^{-1} in the SIMPLISMA trace c of Fig. 9 indicate a very low degree of crystallization of the MoO_3-like compounds if present at all. This low crystallinity results in a very weak Raman cross section relative to that of the Mo_5O_{14}-type oxide.

The statistical SIMPLISMA approach also provides information about changes in the composition of the differently activated samples. The mean spectral weight of each component, i.e. the ratio of each spectral component normalized to the sum of all spectral weights, is a measure of the relative changes of the sample composition as a function of the activation temperature. Fig. 10 shows the relative Raman abundances of the pure spectral components identified in this set of Raman spectra. Of course such an analysis can only give some estimate and does not provide any informa-

tion on absolute concentrations of the different components because the Raman cross sections are inherently unknown. Moreover, the abundance of crystalline MoO_3 remained undetermined because these spectra had to be excluded from this analysis. The inherently unknown Raman cross sections and hence the absolute concentrations are evident when comparing Fig. 10 and Fig. 2. On one hand, Raman spectroscopy has a higher sensitivity toward nanocrystalline, glassy or amorphous materials and reveals structural differences in the starting material which are not comparably detected by XRD. XRD, on the other hand, allows a more reliable determination of the abundance of the crystalline phases. This Raman estimation should therefore be discussed together with the XRD analysis (Fig. 2).
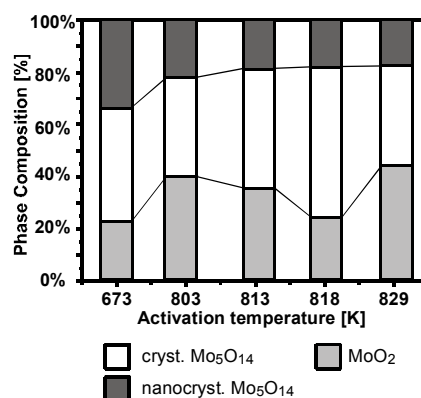

Fig. 10 Normalized spectral weights of the different pure spectral components as determined by SIMPLISMA analysis of the whole set of Raman spectra.

Figure 10 shows the amounts of nanocrystalline Mo_5O_{14}-type oxide, crystalline Mo_5O_{14} and MoO_2 in the MoVW mixed oxide samples as estimated by Raman spectroscopy. The amount of nanocrystalline Mo_5O_{14}, presumably present as oligomeric molybdenum oxide clusters, continuously decreases with increasing activation temperature as expected from the behavior of the XRD amorphous background.

The amount of MoO_2-like mixed oxide increased after treatment at about 803 K in line with the XRD result (Fig. 2). Its relative concentration decreases at higher treatment temperatures at which crystalline Mo_5O_{14}-type material is formed to subsequently increase again. The intermediate higher abundance of MoO_2-type oxide may be related to the formation process of the crystalline Mo_5O_{14}-type material. Kihlborg reports that Mo_5O_{14} can be generated by tempering the respective amounts of MoO_2 and MoO_3 [24].

The amount of crystalline Mo_5O_{14}-type mixed oxide increases at temperatures up to 818 K. Crystallization in general, should lead to a decrease of the FWHM of the Raman bands. Exactly this is observed for the Raman spectra of the Mo_5O_{14}–type mixed oxide. Its amount decreases again at temperatures above 818 K. The XRD results have shown in line with literature [24] that this compound disproportionates at higher temperatures mainly to MoO_2- and MoO_3-type

Mixed molybdenum oxide based partial oxidation catalyst 2. Combined X-ray diffraction, electron microscopy and Raman investigation of the phase stability of (MoVW)5O14-type oxides,
M. Dieterle et al., Journal of Molecular Catalysis A: Chemical, accepted 19 January 2001

10

mixed oxides. Hence, the decreasing Raman abundance of the Mo_5O_{14}-type oxide confirms its disproportionation.

In the Mo_5O_{14}–structure, one third of the MoO_6 polyhedra share two triangular channels, i.e. the MoO_6 polyhedra are strongly deformed. All other MoO_6 polyhedra share only one triangular channel, i.e. these MoO_6 polyhedra are less distorted. Following the analysis of Kihlborg [24], the bond length of the shortest Mo-O bond (in c-direction) in the Mo_5O_{14}–structure is between 1.67 Å and 1.69 Å depending on the distortion of the MoO_6 polyhedron. The number of triangular channels to which a MoO_6 polyhedron is bound, e.g. one or two, determines the second terminal Mo-O bond length (within the ab-plane) to be between 1.85 Å and 1.94 Å, or between 1.71 Å and 1.77 Å, respectively.

Hence, three groups of different bond lengths should be expected for the terminal Mo-O vibrations. One group of Mo-O bonds parallel to the c-axis, and two groups of Mo-O bonds in the ab-plane of the different types of MoO_6 polyhedra with respect to the triangular channels. Exactly these three different Mo-O groups are determined from the experimental Raman spectrum applying the Hardcastle and Wachs model [46] to the Raman bands above 700 cm^{-1}. The bond lengths of the terminal Mo-O bond in c-direction of all MoO_6 polyhedra are estimated to be 1.69 ± 0.02 Å (broad Raman band at 985 cm^{-1}). The bond lengths of the terminal Mo-O bond in the ab-plane of the MoO_6 polyhedra sharing one triangular channel are estimated to be 1.76 ± 0.02 Å (Raman band at 860 cm^{-1}) and 1.77 ± 0.02 Å (Raman band at 845 cm^{-1}). The terminal Mo-O bonds parallel to the ab-plane of the remaining MoO_6 polyhedra are estimated to be 1.8 Å (broad band at 720 cm^{-1}). The remaining band at 902 cm^{-1} not yet being assigned is attributed to the stretching vibration of the terminal Mo-O bond parallel to the c-axis of the MoO_7 pentagonal bipyramids. Although the assignment according to Hardcastle and Wachs model is limited because solid vibrations cannot fully be described in a localized model, the above assignment to certain Mo-O bonds may give a first interpretation of the observed Raman bands of Mo-O valence vibrations, as long as detailed Raman data on single crystals are not available.

Discussion

In the previous paper of this series [37], it was shown that pretreating the sample at 813 K in inert atmosphere results in an increase of the CH_2O yield by factor of 3 with a selectivity of 80%. Oxygen defects were suggested to play a role in the reaction because oxygen richer feed gases led to a decrease of the CH_2O selectivity from 80% to 65% at the unchanged conversion of 99% [37]. XPS and RBS analysis proved oxygen loss from the bulk and surface of the MoVW mixed oxide [37]. The activation also provoked changes of the structure of the MoVW oxide as shown by XRD, Raman spectroscopy and electron microscopy [37].

The starting material was a mixture of nanocrystalline Mo_5O_{14}-type and MoO_3-type oxides [8,37]. After thermal activation, the mixed oxide consisted of a mixture of a majority of Mo_5O_{14}-type oxide a trace amounts of crystalline

MoO_3-type and MoO_2-type oxides [8,37]. The known metastability of Mo_5O_{14} with respect to MoO_3 and MoO_2 [24] explained this result. SEM-EDX and TEM-EDX proved inhomogeneous element distributions. Raman microspectroscopy related this elemental inhomogeneity to a structural inhomogeneity [37].

A core-shell model was developed from the combined results which describes the MoVW active catalyst. It consists of a crystalline core of Mo_5O_{14}-type oxide. The core has a shell of structurally and stoichiometrically ill-defined metal oxide clusters. During partial oxidation catalysis, the crystalline Mo_5O_{14}-type core is suggested to play the role of an electron reservoir for the fast catalytic redox reactions. It also may act as an oxygen buffer due to its open structure of four-, six- and sevenfold coordinated metal ions which allows oxygen and vanadium diffusion as shown by XPS and RBS. Thus, the catalyst is able to adjust to temporary or spatially changing gas phase compositions within the reactor. The shell around the Mo_5O_{14}-type core provides a high number of active sites for the adsorption of the organic substrate and gas phase oxygen.

The combined structural analysis of the MoVW mixed oxide activated at different temperatures, presented in this paper, confirmed this core-shell model. It further revealed that the crystallization of the Mo_5O_{14} type mixed oxide occurs only in a rather narrow temperature range between about 800 and 820 K in inert gas. At activation temperatures above 820 K, the Mo_5O_{15}-type phase increasingly disproportionated into MoO_3 and MoO_2-type oxides. This disproportionation process seemed to occur via a special X-ray amorphous phase, which was termed "bundle" structure according to its appearance in HRTEM images and SAED. This "bundle structure" exhibits ordering only in one dimension and consists of chains of molybdenum oxide polyhedra. These bundles may be an intermediate stage of the reorganization and crystallization of Mo_5O_{14} to MoO_3.

The present study also revealed that a part of the material remained nanocrystalline during thermal activation. This incongruent crystallization behavior of the MoVW mixed oxide most probably is related to the inhomogeneous elemental composition [37]. Mo_5O_{14} tolerates the incorporation of considerable amounts of V and W. Stoichiometries of such phases were reported to be $(Mo_{0.92}V_{0.08})O_{14}$ or $(Mo_{0.75}W_{0.25})O_{14})$, respectively [29,33]. Especially, the incorporation of W favors the formation of Mo_5O_{14}-type oxides comparable with the results on Ta and Nb incorporation [35,36]. Tungsten and vanadium, thus, act as structural promoters enhancing, and stabilizing the formation of the Mo_5O_{14}-type phase. It is known that only 2 to 12% V lead to a stabilization of the Mo_5O_{14} type oxide [29]. The MoVW catalyst however contains 28% vanadium [37] more than the structure tolerates according to literature. It is known on the other hand that Mo_5O_{14} tolerates the incorporation of up to 25% W [32, 33]. The 8% W found in the Mo_5O_{14}-type catalyst hence lead to stabilization of this phase. Alternatively, the role of W and V may also be discussed in view of lattice oxygen defects. The incorporation of oxygen defects into MoO_3 leads to a contraction of the c-axis [2147], hence af-

fect extended regions within the crystal lattice. The promoting effect of V and W may lay in their ability to localize oxygen defects on one hand - V^{5+} prefers fivefold coordination-, and the confinement of these lattice deformations by the redox stable W on the other [48]. In light of this important role of W and V promoters for the stabilization of the Mo_5O_{14}-type mixed oxide, it may be understood why W and V are of paramount importance to the catalytic function. Minor local variations in their concentrations within the material already may lead to different local MoVW oxide phases with different stability regimes and consequently different catalytic behavior.

The Raman characterization of the MoVW mixed oxide catalyst may further shed some light on the role of the different metal-oxygen groups for catalytic action. Generally, it can be said that the shorter the M-O distance is the more basic is the oxygen functionality. Basic, nucleophilic oxygen groups on the catalyst surface are necessary for C-H bond activation [4]. The longer and, therefore, weaker the M-O bond, the easier this oxygen may be inserted into organic molecules. Selective oxidation catalysts have to discriminate for example between α-H atoms of aldehydes and vinylic hydrogen atoms. The key to this selective C-H activation may be seen in the strength of the M-O bond of the active site abstracting the hydrogen. Promoters, e.g. V, Nb, Ta, W, stabilize intermediate Mo oxides with the proper M-O bonds for the selective C-H activation. The second step of selective oxidation, the oxygen insertion into the substrate, is facilitated by weaker M-O bonds which are also present in intermediate oxides. Thus, very strongly bound, basic oxygens will unselectively activate C-H bonds, and very labile M-O groups will lead to total oxidation. The optimization of the catalyst with respect to selectivity and activity may, therefore, be seen as the search for a combination of H-abstracting and oxygen transferring functionalities, e.g. the search of an optimum oxide structure, hence composition of a MoVW intermediate oxide.

The Raman spectra of the Mo_5O_{14}-type oxide contain relevant structural information independent of the crystallinity of the material. With the help of the Hardcastle and Wachs model, Mo-O distances were calculated for the Mo_5O_{14} type oxide which compared well with the crystallographic data. While the nanocrystalline precursor [37], and the amorphous part of the activated sample (Fig. 9b) also showed Raman bands above 930 cm^{-1}, indicating rather short Mo-O bonds, the Mo_5O_{14}-type catalyst has its main Raman features between 840 and 900 cm^{-1}, due to M-O bond distances between 1.77Å and 1.73Å. Pure MoO_3, which is known for total oxidation, has Raman bands in this regime at 995, 820, and 666 cm^{-1}, being due to Mo-O distances of 1.67 and 1.95 Å (according to Hardcastle and Wachs model [46], the bond distance calculated from the band at 820 cm^{-1} cannot be assigned to any distance in MoO_3). MoO_3 thus has much stronger Mo-O bonds on one side – being good C-H bond activators - and much weaker ones on the other, whose oxygens can easily be released leading to an active oxygen insertion function. It must be noted that in situ Raman ^{18}O-labeling experiments of MoO_3 have proven that the ease of oxygen exchange increases with increasing bond length or decreasing bond order [49], supporting the above sketched role of the oxygen transferring M-O groups. A highly active and selective partial oxidation catalyst thus must have optimized oxygen functionalities along with good electron and ion mobilities for fast redox properties (core-shell model). In situ Raman characterization of the MoVW mixed oxide under catalytic action is currently conducted to prove this idea of the different roles of M-O groups in partial oxidation reactions.

Acknowledgement

References

1   J.B. Goodenough, in H. F. Barry, and P. C. H. Mitchell (Eds.), Proc. Climax 4th Int. Conf. on the Chemistry and Uses of Molybdenum, Climax Molybdenum Comp., Ann Arbor, Michigan 1982, p. 1.

2   H. Gruber and E. Krautz, Phys. Stat. Sol. (a), (1980) 615.

3   E. Canadell and M.-H. Wangbo, Chem. Rev., (1991) 965.

4   J. Haber, in H. F, Barry and P. C, H. Mitchell (Eds.), Proc. 4th Inter. Conf. Chemistry and Uses of Molybdenum, Golden, Colorado, Climay Molybdenum Comp., Ann Arbor, Michigan, 1982, p. 395.

5   J. Haber, in G. Ertl, H. Knözinger and J. Weitkamp (Eds.), Handbook of Heterogeneous Catalysis, Vol. 5, Wiley-VCH, Weinheim, 1997, p. 2253ff. Habe Nummer 4 und 5 vertauscht, da das $Cu2(NH_4)_2Mo_3O_{10}$ im Handbuch erwähnt wird!

6   M. Abon, J. Massardier, B. Mingot, J. C. Volta, N. Floquet, and O. Bertrand, J. Catal., 134 (1992) 542.

7   P. Gai-Boyes, Catal. Rev.-Sci. Eng., 34 (1992) 1.

8   H. Werner, O. Timpe, D. Herein, Y. Uchida, N. Pfaender, U. Wild, R. Schlögl, and H. Hibst, Catal. Lett., 44 (1997) 153.

9   A. Magnèli, B. Blomberg, L. Kihlborg and G. Sundkvist, Acta Chem. Scand., 9 (1955) 1382.

10   L. Kihlborg, Adv. Chem., (1981) 36.

11   G. Hägg and A. Magnèli, Ark. Kemi, 19 (1944) 1.

12   A. Magnèli, G. Anderson, B. Blomberg and L. Kihlborg, Anal. Chem., (1952) 1998.

13   A. Magnèli, Acta Cryst., 6 (1953) 495.

14   T. Ekström, E. Salje and R. J. D. Tilley, J. Solid State Chem., 40 (1981) 75.

15   E. Salje, R. Gehlig and K. Viswanathan, J. Solid State Chem., 25 (1978) 239.

16   L. Kihlborg, Acta Chem. Scand., 14 (1960) 1612.

17 A. Magnèli, Acta Chem. Scand., 2 (1948) 861.
18 L. Kihlborg, Acta Chem. Scand., 13 (1959) 954.
19 L. Kihlborg, Ark. Kemi, 21 (1963) 443.
20 L. Kihlborg, Ark. Kemi, 21 (1963) 357.
21 L. Kihlborg, Ark. Kemi, 21 (1963) 471.
22 P. L. Gai-Boys, J. Solid State Chem., (1993) 119.
23 L. A. Bursill, Proc. Roy. Soc., A 311 (1969) 267.
24 L. Kihlborg, Ark Kemi, 21 (1963) 427.
25 B. G. Hyde and M. O'Keefe, Acta Cryst., A29 (1979) 243.
26 L. Kihlborg, Acta Chem. Scand., 14 (1960) 1612.
27 L. Kihlborg, Adv. Chem. Ser., 39 (1963) 37.
28 J. Tichy, Appl. Catal. A, 157 (1999) 363.
29 T. Ekström and M. Nygren, Acta Chem. Scand., 26 (1972) 1827.
30 R. Böhling, A. Drochner, M. Fehlings, D. Knig and H. Vogel, Chem. Ing. Tech., 71 (1999) 3199.
31 H. Böhnke, J.C. Petzold, B. Stein, C. Weimer, and J.W. Gaube, in G. Emig, C. Kohlpaintner, and B. Lücke (Eds.), DGMK Tagungs-bericht 9803, Proc. of the DGMK Conference: "Selective Oxidations in Petrochemistry", Hamburg 1998, DGMK, Hamburg, p.65.
32 T. Ilkenhans, B. Herzog, T. Braun and R. Schlögl, J. Catal., 153 (1995) 275.
33 L. Kihlborg, Acta Chem. Scand., 23 (1969) 1834.
34 K. Brückman, R. Grabowski, J. Haber, A. Mazurkiewicz, J. Slocynski and T. Wiltowski, J. Catal., 104 (1987) 71.

35 T. Ekström and M. Nygren, Acta. Chem. Scand., 26 (1972) 1836.
36 N. Yamazoe and L. Kihlborg, Acta Cryst., B31 (1975) 1666.
37 G. Mestl, Ch. Linsmeier, R. Gottschall, M. Dieterle, U. Wild, and R. Schlögl, J. Mol. Catal A, 162 (2000) 463.
38 R. Böhling, A. Drochner, M. Fehlings, D. König and H. Vogel, Chem. Ing. Techn., 71 (1999) 226.
39 H. Vogel, R. Böhling and H. Hibst, Catal. Lett., 62 (1999) 71.
40 PCW Software, Federal Institute for Materials Research and Testing (BAM), Berlin.
41 W. Windig, Chemometrics & Intelligent Laboratory Systems, 36 (1997) 3.
42 W. Windig and J. Guilment, Anal. Chem., (1991),1425.
43 A. A. Bolzan, B. J. Kenned and C. J. Howard, Aust. J. Chem., 48 (1995) 1473.
44 H. Knözinger and G. Mestl, Top. Catal., 8 (1999) 45.
45 G. Mestl and T. K. K. Srinivasan, Catal. Rev.-Sci. Eng., 40 (1998) 451.
46 F. D. Hardcastle and I. E. Wachs, J. Raman Spectrosc., 21 (1990) 83.
47 M. Dieterle, G. Weinberg and G. Mestl and R. Schlögl, to be submitted.
48 M. Dieterle, G. Mestl and R. Schlögl, in preparation.
49 G. Mestl, P. Ruiz, B. Delmon and H. Knözinger, J. Phys. Chem., 98 (1994) 11269.